Triplet Excitons and Associated Efficiency-Limiting Pathways in Organic Solar Cell Blends Based on (Non-) Halogenated PBDB-T and Y-Series

Jeannine Grüne,* Giacomo Londi, Alexander J. Gillett, Basil Stähly, Sebastian Lulei, Maria Kotova, Yoann Olivier, Vladimir Dyakonov, and Andreas Sperlich*

The great progress in organic photovoltaics (OPV) over the past few years has been largely achieved by the development of non-fullerene acceptors (NFAs), with power conversion efficiencies now approaching 20%. To further improve device performance, loss mechanisms must be identified and minimized. Triplet states are known to adversely affect device performance, since they can form energetically trapped excitons on low-lying states that are responsible for non-radiative losses or even device degradation. Halogenation of OPV materials has long been employed to tailor energy levels and to enhance open circuit voltage. Yet, the influence on recombination to triplet excitons has been largely unexplored. Using the complementary spin-sensitive methods of photo-luminescence detected magnetic resonance and transient electron paramagnetic resonance corroborated by transient absorption and quantum-chemical calculations, exciton pathways in OPV blends are unravelled employing the polymer donors PBDB-T, PM6, and PM7 together with NFAs Y6 and Y7. All blends reveal triplet excitons on the NFA populated via non-geminate hole back transfer and, in blends with halogenated donors, also by spin-orbit coupling driven intersystem crossing. Identifying these triplet formation pathways in all tested solar cell absorber films highlights the untapped potential for improved charge generation to further increase plateauing OPV efficiencies.

J. Grüne, B. Stähly, S. Lulei, M. Kotova, V. Dyakonov, A. Sperlich
Experimental Physics 6
Julius Maximilian University of Würzburg
Am Hubland, 97074 Würzburg, Germany
E-mail: sperlich@physik.uni-wuerzburg.de
J. Grüne, A. J. Gillett
Cavendish Laboratory
University of Cambridge
JJ Thomson Avenue, Cambridge, UK
E-mail: jg2082@cam.ac.uk
G. Londi, Y. Olivier
Laboratory for Computational Modeling of Functional Materials
Namur Institute of Structured Matter
University of Namur
Rue de Bruxelles, 61, 5000 Namur, Belgium

1. Introduction

Organic solar cells (OSC) based on non-fullerene acceptors (NFAs) have attracted much attention due to their strong absorption in the visible and near infrared spectral regions and their energy-level tunability, in contrast to fullerene acceptors.[1] However, despite the great success of OSC development to power conversion efficiencies (PCE) up to 19%,[2] there is still untapped potential for further improvement. One limiting factor is the total voltage loss ($\Delta V_{loss} = q^{-1}E_g - V_{OC}$), defined as the difference between the optical bandgap (E_g) and the open-circuit voltage (V_{OC}).[3–6] Besides, ΔV_{loss} is composed of losses due to radiative (ΔV_r) and non-radiative (ΔV_{nr}) recombination.[4,7] According to the Shockley–Queisser limit, an ideal solar cell possesses only radiative recombination, making the contribution ΔV_r unavoidable.[8,9] Non-radiative recombination processes thus reduce V_{OC} and the short-circuit current and are therefore of great interest for OSC research.[3,5] Furthermore, after optical excitation of donor (D) or acceptor (A) moieties, charge transfer (CT) at the interface is expected to reduce the photovoltage due to the difference in the D or A bandgaps and the energy of CT states ($E_{g}- E_{CT}$).[6,10,11] However, in state-of-the-art D:A combinations, such as PM6:Y6, this difference is almost negligible, making non-radiative recombination the most dominant in terms of efficiency losses.[7]

Due to the close energetic alignment between NFA singlet states and the CT states, especially in the PBDB-T:Y-series blends, NFA triplet states are energetically located below the CT states and represent a significant non-radiative decay channel for excitons.[12] Preventing the population of these triplet states is extremely difficult, even in state-of-the art blends as shown in this work. Direct intersystem crossing (ISC) from optically excited donor or acceptor singlet states to molecular triplet states is one of the possible triplet formation mechanisms.[13,14] The yield of this geminate pathway depends on the number of optically generated singlet excitons not reaching the D:A interface within their exciton diffusion length to undergo charge transfer.[15,16] Another loss pathway is due to triplet CT states

**ADVANCED
SCIENCE NEWS**
www.advancedsciencenews.com

**ADVANCED
FUNCTIONAL
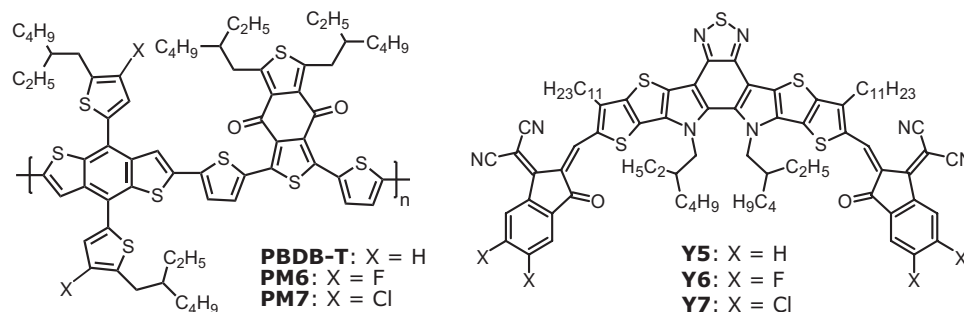MATERIALS**
www.afm-journal.de

Figure 1. Chemical structures of studied organic solar cell materials. As donors PBDB-T (X = H), fluorinated version PM6 (X = F, also called PBDB-T-2F) and chlorinated version PM7 (X = Cl, also called PBDB-T-2Cl) are investigated. Acceptors represent Y5 (X = H, also called BTP), Y6 (X = F, also called BTP-4F) and chlorinated version Y7 (X = Cl, also called BTP-4Cl).

that relax spin-allowed to energetically lower molecular triplet states, also called electron or hole back transfer (EBT, HBT).[3,17] In polymer- or fullerene-based blends, triplet states are thereby often formed not by ISC from the S_1 state but instead by geminate back transfer directly following the charge transfer.[18,19] In newer materials, such as NFA-based blends, HBT from CT states formed after non-geminate recombination was shown to have a considerable impact by limiting V_{OC}.[3] All triplet formation mechanisms can lead to triplet excitons, which are localized on the lowest-lying molecular triplet states and thus increase non-radiative recombination.

In the present work, we set the focus on the impact of donor and acceptor halogenation on the formation of triplet excitons. Halogenation of, e.g., donor polymers can improve device efficiencies, as shown for fluorination and chlorination of PBDB-T to yield PM6 and PM7, respectively.[20–22] Thereby, halogenation is beneficial in terms of PCE, since it stabilizes the highest occupied molecular orbital (HOMO) energy level, resulting in increased V_{OC}.[20,23] However, the question arises whether the reduced HOMO offset impacts the important hole transfer process in NFA blends. Another advantage of halogenation is observed for morphology since halogenation increases the molecular planarity and ordering. This in turn results in improved aggregation and larger domain sizes, leading to a rise in charge carrier mobility and in fill factor but could also lead to undissociated singlet excitons that undergo ISC.[24] Additionally, ISC rates of organic semiconductors could be enhanced substantially by halogenation as shown for organic light-emitting diodes (OLEDs) employing thermally activated delayed fluorescence (TADF), where bromination or iodination increases reverse ISC rates due to the heavy atom effect.[23] In this context, it remains to be clarified whether fluorination and chlorination of OPV materials also have an impact on ISC and hole transfer kinetics or overall on triplet exciton formation.

Since formation of long-lived triplet states results in a loss of OSC performance and can exacerbate device degradation, studying the presence of triplet excitons and their generation mechanisms is essential. We used two complementary methods, which are highly sensitive to triplet excitons: photoluminescence detected magnetic resonance (PLDMR) and transient electron paramagnetic resonance (trEPR). Both methods were often applied independently of each other in the past to investigate triplet formation in OSCs.[3,25–28] Especially the combination of both techniques has been shown to be very

powerful: trEPR probes triplet excitons directly by detection of microwave absorption between triplet sublevels occurring during resonance transitions and reveals highly spin-polarized, i.e., geminate triplet exciton formation pathways, such as ISC or geminate HBT.[29] In contrast, PLDMR probes triplet states indirectly with the higher sensitivity of optical detection and thus reveals those spin states that are associated with luminescence, e.g., via triplet–triplet annihilation (TTA), ground state depletion or (reverse) ISC.[30,31] PLDMR is therefore well suited to detect long-lived triplet excitons including those formed by non-geminate recombination and identify their molecular localization.[26,27] To further study the influence of halogenation on excited state kinetics, including hole transfer and ISC rate constants, we performed transient absorption (TA) measurements and quantum-chemical (QC) calculations. By the combination of these complementary techniques, we thoroughly investigated the spin physics of state-of-the-art donor and acceptor materials in different combinations: the polymer PBDB-T and its halogenated (i.e., fluorinated and chlorinated) variants PM6 and PM7, as well as the respective NFAs Y6 and Y7 (**Figure 1**, whereby Y5 is used for comparison of (non-) halogenation in QC calculations).

2. Probing Triplet Excitons with Magnetic Resonance

Triplet excitons (either CT or molecular) are characterized by two interacting electron spins, whose fundamental spin physics is briefly described in the following. The corresponding Hamiltonian operator in X-band regime (microwave frequency $v_{MW} \approx 9.4$ GHz and external magnetic field $B_0 \approx 340$ mT) can be reduced to mainly three contributions: the electron Zeeman (EZ) interaction $\hat{H}_{EZ}$, zero-field splitting (ZFS) $\hat{H}_{ZFS}$ and exchange interaction $\hat{H}_{EX}$ (other contributions, including hyperfine fields, can be considered as negligible perturbations):[32]

$$\hat{H} = \hat{H}_{EZ} + \hat{H}_{ZFS} + \hat{H}_{EX} = \mu_B \vec{B}^T \mathbf{g} \hat{\vec{S}} + \hat{\vec{S}}^T \mathbf{D} \hat{\vec{S}} + \hat{\vec{S}}_1^T \mathbf{J} \hat{\vec{S}}_2 \tag{1}$$

Here, $\hat{\vec{S}}$ is the total spin angular momentum operator (with $\hat{\vec{S}}_1$ and $\hat{\vec{S}}_2$ being the operators for the respective electron spins), $\mathbf{g}$ the g-tensor (assumed to be isotropic due to a small spin-orbit coupling (SOC) in organic molecules), μ_B the Bohr

magneton, D the ZFS tensor and J the exchange-interaction tensor. The Zeeman interaction describes the quantized splitting of the paramagnetic states into their sublevels with spin quantum numbers $m_s = +1, 0, –1$, i.e., the spin Hamiltonian eigenstates $|T_+\rangle$, $|T_0\rangle$ and $|T_-\rangle$, based on the interaction with the external magnetic field $\vec{B}$.[33] For nearby electron and hole (i.e., a locally excited state on a given molecule), the triplet sublevels are already energetically split in absence of an external magnetic field due to dipolar interactions between the spins of the unpaired electrons. This splitting is referred to as ZFS with the two scalar parameters D and E of the corresponding ZFS tensor D: the axial parameter D is related to the average inter-spin distance r (to first order approximation $D \sim r^{-3}$), whereby E describes the rhombicity, thus the deviation from axial symmetry.[32,34,35] For CT states with larger spin–spin distances than those of molecular states, spin conservation during charge separation generates spin-correlated radical pairs (SCRP) with exchange J and dipolar interaction D being in a comparable range. The Hamiltonian eigenstates are then represented by pure $|^3CT_-\rangle$ and $|^3CT_+\rangle$ triplet states ($m_s = \pm1$) and two mixed singlet-triplet states $|^3CT_0\rangle$ and $|^1CT_0\rangle$ ($m_s = 0$), whereby due to angular momentum conservation, only a spin mixing between the latter two can occur. Further information about triplet spin states is given in SI.

2.1. Detecting Triplet Excitons with Spin-Sensitive Photoluminescence

Figure 2a depicts the PLDMR principle of probing the PL change of singlet states (either CT or molecular), which are coupled (via TTA, ISC, etc.) with paramagnetic states.[28] Microwave irradiation induces transitions between the sublevels (purple arrows) leading to a change in PL intensity. In the case of $|^3CT\rangle$ states, the comparatively large inter-spin distance results in negligible dipolar interaction (negligible D value), which in turn induces a symmetrical splitting of triplet sublevels $|^3CT_+\rangle$, $|^3CT_0\rangle$ and $|^3CT_-\rangle$ in a magnetic field. Microwave irradiation of frequency ν_{MW}, resonant to the energetic

sublevel splitting, induces spin-allowed $\Delta m_s = \pm1$ transitions at closely spaced magnetic field values. The result is a change of steady-state triplet population, leading to an increased ($\Delta PL/PL > 0$) or reduced ($\Delta PL/PL < 0$) PL yield under resonance conditions, referred to as full-field (FF) signal. For the case of a localized molecular triplet ($|T_{mol}\rangle$ in Figure 2a), the ZFS results in an asymmetric splitting of the triplet sublevels in the applied magnetic field. Thus, microwave irradiation induces transitions and PL changes at more widely spaced magnetic field values, the distance of which depends linearly on the ZFS parameters D and E. In addition, there is a certain probability of $\Delta m_s = \pm2$ transitions at half of the resonant magnetic field, referred to as half-field (HF) signal.[34] The intensity of the HF signal increases quadratically with D (intensity $\sim D^2 \sim r^{-6}$) and is therefore detectable for molecular triplet excitons only.[36] The ZFS parameter D, related to the total width of the spectrum ($|2D|/g\mu_B$), together with the spectral position of the HF signal allows for the molecular localization of the triplet states involved in the PL generation process to be readily determined.[27]

Figure 2b presents PLDMR spectra of the pristine materials PM6 and Y6 as well as of blends of Y6 with the polymer donors PBDB-T, PM6, and PM7. The measurements were performed for thin-film samples produced by an optimized spin-coating recipe comparable to OSC device production (recipe given in Experimental Section, measurements for drop-cast samples in EPR tubes are shown in Figures S11 and S12, Supporting Information).[37,38] The PLDMR spectra of the pristine polymers are almost identical; the spectrum of PM6 is shown here while the spectra of PBDB-T and PM7 can be found in Figure S9 (Supporting Information). All polymer spectra show a broad molecular triplet feature with $D/h = 1500$ MHz (110 mT width) and a HF signal at $B = 165$ mT. Pristine NFA Y6 shows a molecular triplet signal with a smaller D value of $D/h = 950$ MHz (70 mT width) and a HF signal at $B = 166.8$ mT. Spectral simulation parameters derived by the MATLAB toolbox EasySpin[39] are summarized in Table S5 (Supporting Information). PLDMR spectra of all neat materials show additional central narrow peaks, which in polymers are generally assigned to photo-generated polaron pairs.[40–43] Neat NFAs, as Y6 or ITIC, show
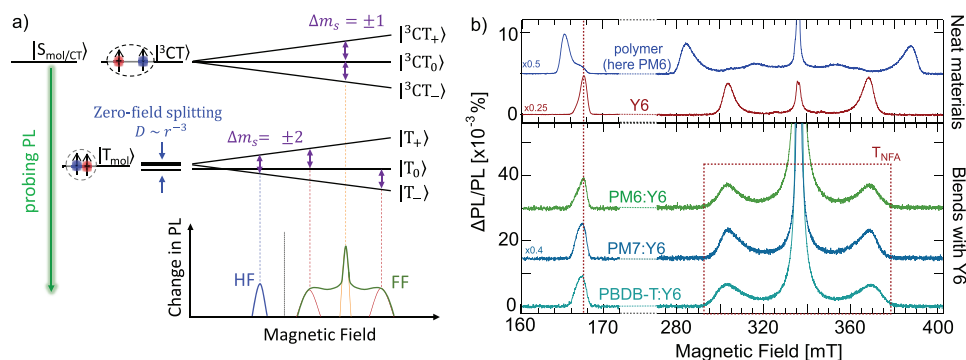

Figure 2. Photoluminescence detected magnetic resonance (PLDMR) of triplet excitons. a) PLDMR probes PL changes of singlet states ($|S_{mol/CT}\rangle$), which are coupled to paramagnetic triplet states. CT and molecular triplet states ($|^3CT\rangle$, $|T_{mol}\rangle$) are split due to Zeeman and ZFS interactions: $|^3CT_{+,0,-}\rangle$, $|T_{+,0,-}\rangle$. Microwave irradiation induces $\Delta m_s = \pm1$ transitions (purple), leading to a change in the PL yield detected as full field spectrum (FF). An additional signal is detected at half the magnetic field (HF) for $\Delta m_s = \pm2$ transitions. b) PLDMR spectra for neat materials PM6 and Y6 as well as the blends PBDB-T:Y6, PM6:Y6, and PM7:Y6. The spectral width of the FF signal and the position of the HF signal are determined by the material-dependent ZFS and therefore the triplet excitons in the blends can be assigned to the NFA Y6 (red dotted box). All PLDMR measurements used $\lambda_{ex} = 473$ nm for excitation of donor and acceptor and were performed at $T = 10$ K.

negligible photogeneration of polarons, as evidenced by light induced EPR (LEPR), suggesting short-lived (intermolecular) excited states with weak dipolar interactions, such as SCRPs, being the origin of the central peak in PLDMR.[42–44] When blending Y6 with the donors PM6, PM7, and PBDB-T (lower traces), the intensity of the central peak increases significantly due to the increased formation of separated polaron pairs and spectrally overlapping D:A interfacial CT states. Since PLDMR is performed on thin films without electrodes, all formed CT states and polaron pairs do eventually recombine. By means of trPLDMR, we can assign the PLDMR response of the NFA triplet and CT states to be positive (Figure S10, Supporting Information), mostly stemming from annihilation processes such as TTA or triplet-polaron annihilation (TPA).[26,45,46] Indeed, TPA was found to be one of the dominant bimolecular interactions in PM6:Y6, responsible for significant voltage losses.[3,41,47]

All three blends show a broad triplet feature (300–370 mT) arising from long-lived molecular triplet excitons. The axial ZFS parameter D, i.e., the width of the FF spectra, and the positions of the HF signals at 166.8 mT (dotted vertical line) clearly assign these PLDMR features to triplet excitons on the NFA Y6. The D value in the blends is slightly larger with $D/h = 1020$–1040 MHz (Table S5, Supporting Information) than in neat Y6 due to a marginally different molecular packing. However, the spin density delocalization is not strongly affected according to the relation $D \sim r^{-3}$. Furthermore, the triplet features in all PLDMR spectra can only be simulated taking considerable molecular ordering into account, leading to pronounced spectral "wings".[39,48] The ordering factor λ_Θ gives information about the preferred molecular orientation relative to the external magnetic field, defined by the angle Θ. Neat Y6 shows a clear preferential alignment of the molecules (Table S5, Supporting Information), in line with intermolecular face-on stacking and face-on stacking on the substrate, as evidenced by GIWAXS.[49–51] When blending Y6 with the polymers, the ordering is comparable for all blends (Table S5, Supporting Information). The preferential orientation of Y6 molecules in the blends supports that the backbone ordering known for neat Y6 is maintained when blended with the polymer, as already confirmed for PM6:Y6 by GIWAXS measurements.[52] The

PLDMR spectra suggest similar preferential orientation of Y6 also with PBDB-T and PM7, whereby this face-on orientation in the blend is shown to be beneficial for charge transport in the direction normal to the substrate surface.[53,54]

The triplet excitons detected on the NFA can be generated either by direct ISC, non-geminate HBT or by geminate HBT. Although PLDMR is not able to distinguish between these formation mechanisms, its high sensitivity is crucial to reveal the presence of triplet excitons generated by all efficiency-limiting pathways. This sensitivity is achieved due to the optical detection and the continuous illumination, enhancing spin polarization due to annihilation effects.[29] PLDMR measurements were also performed with NFA Y7 (Figure S12, Supporting Information), where triplet excitons were found on Y7. Hence, we observe molecular triplet excitons in all studied OPV blend, localized on the NFA.

2.2. Probing Triplet Pathways with Transient EPR

While PLDMR probes steady-state populations under continuous illumination, trEPR probes short-lived spin polarization generated by pulsed laser excitation. Thereby, trEPR is able to reveal generation pathways of geminate triplet excitons with distinct spin polarization due to specific mechanisms, such as ISC.[33,34] As discussed below, the fraction of these geminate triplet excitons is very low in the studied blends. For the spin-coated samples, this yields a signal that is detectable but too weak to determine the spin polarization pattern with confidence (Figure S2, Supporting Information). Therefore, trEPR measurements were additionally performed on drop-cast samples (**Figure 3**), which yielded a better signal-to-noise ratio to reliably identify the population mechanism (see Supporting Information).

Figure 3a shows the trEPR spectrum of Y6 and its blends with the three donor polymers (trEPR of pristine polymer donor as well as blends with Y7 are shown in Figures S15 and S16, Supporting Information). Neat Y6 shows a 70 mT wide spectrum, corresponding to $D/h = 945$ MHz, similar to the value obtained with PLDMR ($D/h = 950$ MHz). When blending
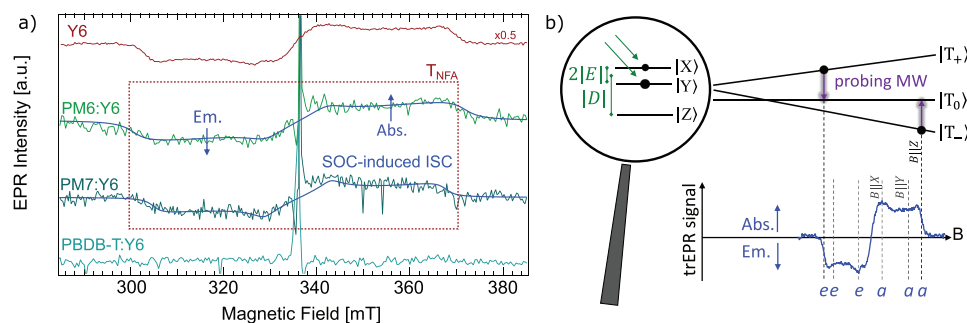

Figure 3. trEPR spectra of pristine Y6, PM6:Y6, PM7:Y6, and PBDB-T:Y6. a) trEPR spectra of blends with the halogenated donors (PM6 and PM7) have the same spectral fingerprint as triplets on pristine Y6 (red dotted box) as shown by the spectral fits (blue). The blend of PBDB-T:Y6 shows no detectable triplet formation. b) Formation of polarized trEPR spectra for spin-orbit coupling (SOC) driven ISC triplets. ISC is sublevel selective and acts on the zero-field sublevels $|X\rangle$, $|Y\rangle$ and $|Z\rangle$. These populations are converted into high-field populations $|T_+\rangle$, $|T_0\rangle$, and $|T_-\rangle$, depending on the three principal axes orientation of the ZFS tensor $\mathbf{D}$ with respect to magnetic field $\vec{B}$. Microwave emission (e) or absorption (a) for $\Delta m_s = \pm1$ transitions (purple) results in the shown Y6 trEPR pattern (blue). The $eeeaaa$ polarization pattern is due to SOC-driven ISC. All trEPR measurements used $\lambda_{ex} = 532$ nm for excitation of donor and acceptor and were performed at $T = 10$ K.

Y6 with the polymers, all blends show an additional intense middle signal with narrow microwave emission/absorption feature ($B = 336.5$ mT), corresponding to interfacial CT states and photogenerated polarons. The width correlates with that of PLDMR middle features in Figure 2b, assigning both to the same $|^3CT\rangle$ states. Regarding the molecular (broad) trEPR feature, almost identical spectral fingerprints are detected for the blends of PM6:Y6 and PM7:Y6. The same spectral width proves the signals are also arising from Y6 triplet excitons as already shown with PLDMR. In contrast to PLDMR, trEPR spectra exhibit no visible molecular ordering, even in the spin-coated blends.[29] This is attributable to the fact that trEPR probes all (highly) spin-polarized triplet excitons, while PLDMR probes predominantly those triplets that are associated with luminescence, e.g., via more dominant TTA in crystalline phases as a result of an increased diffusion length.[29,55,56] The polarization pattern of the trEPR signal of PM6:Y6 and PM7:Y6 displays an *eeeaaa* signature, i.e., microwave emission at lower and microwave absorption at higher fields, consistent with triplet excitons populated by the geminate pathway of SOC-driven ISC.

Regarding PBDB-T:Y6, molecular triplet excitons on Y6 are detected with PLDMR (Figure 2b), whereby no molecular triplet feature in trEPR is observed. While trEPR probes geminate triplet excitons only, PLDMR is also sensitive to triplet excitons formed by non-geminate recombination. This finding assigns the triplet excitons in PBDB-T:Y6 visible in PLDMR (Figure 2) to non-geminate HBT. As also discussed below, non-geminate triplet excitons represent the main contribution of energetically trapped triplet excitons. Thus, the triplet yield visible in trEPR is overall a very minor triplet channel but important to prove the mechanism of present SOC-driven ISC.

Figure 3b shows the formation of the trEPR spectral pattern of the spin-polarized triplet feature of the neat materials and the blends. It arises by the selective population of the triplet sublevels by ISC from the excited singlet states.[34] This ISC mechanism for molecular excitons with small wave function extent (large D value) is based on SOC, which is dominant for small electron-hole distances.[57] At larger inter-spin distances, SOC is negligible and (reverse) ISC is driven by hyperfine interactions (HFI) leading to different trEPR spectral patterns for, e.g., triplet excitons formed via geminate HBT, discussed further in the SI.[3,58] SOC-driven ISC acts on the zero-field triplet states, given by the eigenstates $|X\rangle$, $|Y\rangle$, and $|Z\rangle$ of the Hamiltonian (where X, Y, and Z are the principal axes of the ZFS tensor **D**), which are split due the ZFS parameters D and E.[32,33] The ISC rate depends on the difference in the nature of the singlet and triplet excited states involved in this process, whereby the population is spin selective, depending on the symmetries of the excited singlet and triplet wave functions.[33,34,59,60] In the studied materials, SOC-driven ISC leads to a relative population p_i of zero-field triplet sublevels, in, e.g., neat Y6 of $[p_z, p_y, p_x] = [0, 0.66, 0.34]$ (see Section 6 and Table S7, Supporting Information). In a magnetic field, the population of the corresponding high-field sublevels $|T_+\rangle$, $|T_0\rangle$, $|T_-\rangle$ can be derived from the zero-field population, which depends on the orientation of the ZFS tensor with respect to the external magnetic field (here shown for $\vec{B} \| Z$, further details in Figure S13, Supporting Information).[33] In this projection, the $|T_+\rangle$ and $|T_-\rangle$ states are more populated than $|T_0\rangle$, with resonant microwave irradiation driving this imbalance toward equal distributions. Together with the asymmetric splitting due to ZFS, microwave emission (*e*) at lower fields (negative intensity) and enhanced absorption (*a*) at higher fields (positive intensity) can be detected with trEPR.[34] In disordered organic samples, transitions from all orientations of **D** with respect to $\vec{B}$ are superimposed as a characteristic spectrum with *eeeaaa* pattern, which is indicative for triplet excitons populated by SOC-driven ISC (Figure S13, Supporting Information).[33] Returning to Figure 3a, the SOC-driven ISC pattern of Y6 triplets is also present in the blends of PM6:Y6 and PM7:Y6 with similar zero-field population of triplet sublevels as neat Y6 (Table S7, Supporting Information), indicating ISC on the NFA.

3. Influence of Halogenation on Excited State Kinetics

3.1. Hole Transfer in (Non-) Halogenated PBDB-T:Y-Series Studied by Transient Absorption

Figure 4 shows TA spectra and hole transfer kinetics for Y6 blends with excitation wavelength of 800 nm for selective excitation of the NFA Y6 (blends with Y7 discussed in Section 3 of Supporting Information). The low fluence of ≈ 0.6 μJ cm^{-2} used in the TA measurements on the blends prevents excess bimolecular recombination in the first few nanoseconds from affecting the determination of the hole transfer timescales.

Figure 4a shows the time dependent TA spectra of PBDB-T:Y6; TA spectra for PM6:Y6 and PM7:Y6 are shown in Figure S1 (Supporting Information). The Y6 ground state bleach (GSB) centered at 830 nm and photo-induced absorption (PIA) of Y6 singlet excitons at 910 nm are observed immediately after optical excitation.[44,61] In addition, a clear GSB at 580–650 nm emerges in the TA spectra, consistent with the absorption spectrum of the polymer.[62,63] Since the excitation pump does not generate excitons on PBDB-T (PM6 and PM7, respectively), the appearance of the polymer GSB indicates dissociation of Y6 excitons via hole transfer at the D:A interface. The presence of the polymer GSB already at 0.2 ps in all blends suggests that some ultrafast hole transfer occurs.[61,64] However, as the Y6 GSB falls, likely due to some spectral overlap with the negative sign PIAs of Y6 electron and PM6 hole polarons forming at 780 and 920 nm,[65] respectively, the polymer GSB continues to increase, peaking ≈100 ps. This indicates that a significant population of the NFA excitons require additional time to dissociate. On similar timescales, another broad negative band grows in between 680 and 730 nm. This has previously been assigned to the electro-absorption of the donor polymer PM6, indicating the separation of bound interfacial CT states into free charges.[3,61,65] However, while all blends with the NFA Y6 show a considerable hole transfer yield, it decreases upon halogenation of the donor in these blends (Figure S1, Supporting Information) and with NFA Y7 (Figure S4, Supporting Information), further discussed below and in Sections 2 and 3 of Supporting Information.

Figure 4b shows the normalized hole transfer kinetics from the polymer GSB between 580 and 650 nm. The hole transfer rate appears to be comparable for all donor combinations
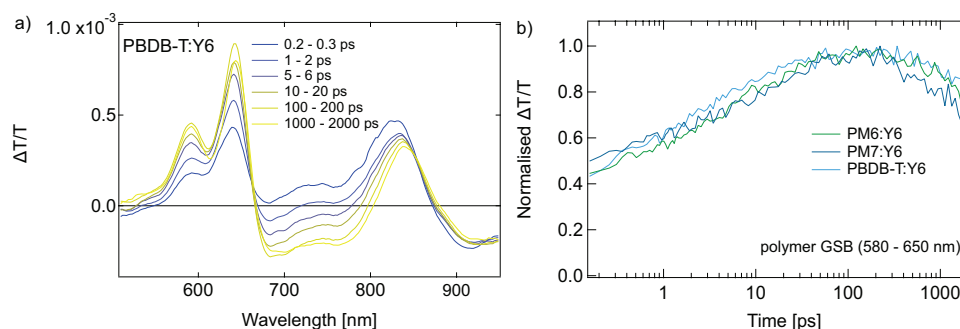
Figure 4. Transient absorption (TA) measurements. a) TA spectra at different time delays for PBDB-T:Y6. b) Hole transfer kinetics extracted from polymer ground state bleach GSB (580–650 nm) for PM6:Y6, PM7:Y6, and PBDB-T:Y6. In all samples, hole transfer takes place on comparable time-scales. All TA measurements used a pump pulse wavelength of 800 nm for selective excitation of Y6 and were performed at $T = 293$ K.

(PBDB-T, PM6, and PM7) with Y6. In addition to the ultrafast component already visible at 0.2 ps, the hole transfer yield increases up to a peak at 100 ps, indicating that the hole transfer is completed. Donor combinations with NFA Y7 (Figure S4, Supporting Information) also show very similar hole transfer kinetics to Y6 blends. The slower hole transfer rate component is often attributed to diffusion limitations for excitons created far from the D:A interface.[66,67] Zhong et al. performed measurements on 5:1 polymer:NFA blends to disentangle the ultrafast component, determined by intrinsic CT rates, from the morphology dependent exciton diffusion rates.[64] However, the studied blends show similar kinetics in both components, reflecting that neither the small energetic shift in HOMO level (Figure S17, Supporting Information) nor probable morphology differences upon halogenation have a significant impact on the hole transfer rates, which has been found to be largely governed by the interfacial morphology in PM6:Y6.[61] Interestingly, despite initially generating a similar number of excitations on Y6 (as seen by the equal intensity of the Y6 GSB at 0.2 ps in all blends), the intensity of the polymer GSB reaches the highest value in PBDB-T, followed by PM6 and then PM7 (Figure S1, Supporting Information). This indicates a difference in the absolute hole transfer yield, implying that a smaller number of Y6 excitons reaches the D:A interface for hole transfer.

3.2. SOC-driven ISC in (Non-) Halogenated Y-Series by Quantum-Chemical Calculations

Singlet excitons formed upon photoexcitation that do not reach the D:A interface for efficient hole transfer may eventually undergo ISC to the respective triplet states. We performed QC calculations to assess possible differences in the ISC rates due to halogenation. In the assessment of the energetic landscape of the investigated donor polymers and the NFA Y-series, singlet and triplet vertical excitation energies were computed by means of screened range-separated hybrid (SRSH) time-dependent DFT calculations, performed within the Tamm–Dancoff approximation (TDA) (see Supporting Information for further details and Table S2, Supporting Information).[68,69] In order to obtain triplet energies, the theoretical singlet-triplet energy gap ΔE_{ST} was subtracted from experimental singlet energies (Table S2, Supporting Information). Then we focused

on the calculation of ISC rates k_{ISC} for the NFA Y-series and we resorted to the semi-classical Marcus–Levich–Jortner expression, which treats high-frequency intramolecular vibrational modes in a quantum-mechanical fashion:

$$k_{ISC} = \frac{2\pi}{\hbar} \left| \left\langle T_x \left| \hat{H}_{SOC} \right| S_1 \right\rangle \right|^2 \sqrt{\frac{1}{4\pi\lambda_s k_B T}}$$
$$\times \sum_n \left\{ \exp(-S) \frac{S^n}{n!} \times \exp\left[-\frac{\left(-\Delta E_{S1-Tx}^0 + \lambda_s + n\hbar\omega \right)^2}{4\lambda_s k_B T} \right] \right\} \quad (2)$$

Here, $\left| \left\langle T_x \left| \hat{H}_{SOC} \right| S_1 \right\rangle \right|$ displays the SOC matrix element involved in the ISC process from $|S_1\rangle$ to the manifold of the triplet states $|T_x\rangle$, whose energy differences are given by ΔE_{S1-Tx}^0; λ_s is the external reorganization energy (set in a range between 0.05 and 0.2 eV); $\hbar$ is the reduced Planck's constant; k_B is the Boltzmann constant; and T is the temperature (set at 298 K). $\hbar\omega$ is the energy of an effective high-frequency intramolecular vibrational mode (0.15 eV of a carbon–carbon stretching) that assists the ISC and $S = \lambda_i / (\hbar\omega)$ is the Huang–Rhys factor, which is a measure of the electron–phonon coupling assisting the ISC process and λ_i the internal reorganization energy.

The nature of $|S_1\rangle$ excited state of Y6 and Y7 is very similar to that of $|T_1\rangle$ excited state that makes SOC between these excited states negligible according to the El-Sayed's rule.[70,71] For instance, in Y6 both $|S_1\rangle$ and $|T_1\rangle$ show a dominant HOMO-to-LUMO transition (98% for $|S_1\rangle$ and 90% for $|T_1\rangle$, in agreement with literature,[72] see Figure S7 (Supporting Information) leading to a very small SOC value (<0.05 cm^{-1}). In contrast, the $|T_2\rangle$ excited state (which is energetically also below $|S_1\rangle$) shows a contribution of 75% of HOMO-to-LUMO+1 transition, involving a different localization of the electron wave function (see Figure S7, Supporting Information) in comparison to $|S_1\rangle$. Consequently, SOC between $|S_1\rangle$ and $|T_2\rangle$ is much larger (on the order 0.1 cm^{-1}) compared to the SOC between $|S_1\rangle$ and $|T_1\rangle$, enabling singlet-triplet conversion by ISC on the NFAs.

Moreover, to study the influence of halogenation, we compared Y6 and Y7 together with the non-halogenated version Y5. The same natural transition orbitals (NTOs) were found in all three cases, meaning that the relevant low-lying excited states (namely $|S_1\rangle$ and $|T_2\rangle$) have the very same nature and halogenation does not play a key role here. In fact, the electron density

on the halogen atoms in the NTO is negligible (Figure S7, Supporting Information), resulting in the SOC matrix element being almost insensitive to halogenation. As the respective ΔE_{ST} is also not changing considerably (Table S2, Supporting Information) and, additionally, has been shown to have a minor influence on the ISC rate, the SOC-driven ISC kinetics from $|S_1\rangle$ via $|T_2\rangle$ can be assumed to be comparable for all (non-) halogenated acceptors.

4. Discussion

Figure 5 shows the Jablonski diagram of the studied PBDB-T:Y-series blends. All energies and observed triplet formation mechanisms are summarized in Table S1 (Supporting Information). Given the low HOMO offset in all investigated blends, the low-lying NFA singlet states possess a small energetic offset to CT states, allowing small energy losses in comparison to fullerene-based solar cells.[5,44] However, given a large ΔE_{ST} of molecular states (≈0.5–0.6 eV), the small singlet offset results in the lowest NFA triplet being energetically below the CT states. Such a large ΔE_{ST} prevents efficient triplet harvesting mechanisms, such as thermal upconversion, to directly return to the interfacial CT states and to yield photocurrent. Without further interactions, triplets are instead energetically trapped and, given the small first order decay rates to singlet ground states, can be detected by both PLDMR and trEPR.[3,29] The fact that triplet excitons were detected in all PBDB-T:Y-series blends should draw attention to the role of the triplets in the solar cell power loss that results in a direct consequence of the energetic reduction of the HOMO offset.[3] However, to be able to control the population of these triplet states, we studied in detail the
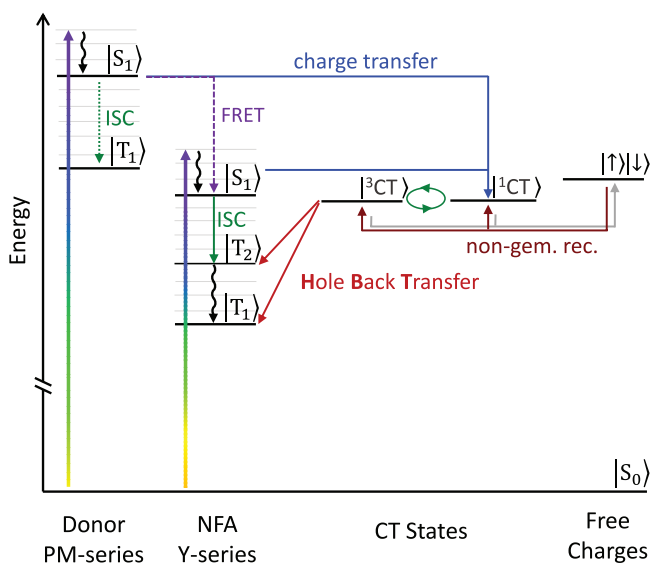

Figure 5. Energy diagram of the studied OPV blends. Optical excitation of donor or acceptor singlet is followed by interfacial charge transfer, FRET or direct ISC. NFA triplet states ($|T_1\rangle$, $|T_2\rangle$) are energetically below the intermolecular CT states ($|^1CT\rangle$, $|^3CT\rangle$) and therefore represent energetic trap states. NFA triplet states are populated by ISC from the NFA $|S_1\rangle$ state or by HBT from $|^3CT\rangle$, which itself is populated by non-geminate recombination of free charges.

photophysical processes and pathway differences between the state-of-the-art (non-) halogenated donor and acceptor blends, which surprisingly highlights the non-halogenated donor PBDB-T. In the following, we discuss the different pathways affecting the population of the triplet states (direct ISC from $|S_1\rangle$ states upon photoexcitation as well as HBT from $|^3CT\rangle$ states formed via either geminate or non-geminate recombination) and the impact of halogenation on the major kinetic rates.

4.1. Triplet Formation by Geminate and Non-Geminate Pathways

Triplet excitons were detected in all PBDB-T:Y-series blends on the NFA triplet states via PLDMR (Figure 2 and Section 5, Supporting Information). In trEPR (Figure 3), probing predominantly geminate excitons, the polarization patterns for the detected triplets with donors PM6 and PM7 are consistent with polarization for SOC-driven ISC triplets (*eeeaaa*). These direct ISC-driven triplet states can be clearly distinguished from other triplet formation processes, such as HBT from $|^3CT\rangle$ states formed via geminate recombination as observed to be a dominant process in polymer:fullerene blends.[16,29] However, in the investigated NFA-based blends, no indication of geminate HBT could be observed, ruling out this triplet formation mechanism, consistent with reports in the literature.[3] The comparable zero-field populations of the blends and neat Y6 (see Section 6 and Table S7, Supporting Information) indicate that ISC takes place on the NFA, e.g., in the center of NFA domains larger than the exciton diffusion length away from the D:A interface. QC calculations revealed the SOC-driven ISC rate is increased by the presence of higher-lying triplet states with larger variation in their nature with respect to $|S_1\rangle$, enhancing the SOC matrix element. As for the donor, ultrafast electron transfer quenches the singlet excitation in the sub-picosecond timescale, with the possibility of Förster resonance energy transfer (FRET) to the NFA as another deactivation channel, suggesting the yield of excitons undergoing ISC on the donor to be negligible (dotted arrow in Figure 5).[11,61,67,73] Furthermore, donor triplet levels are energetically above the CT and NFA states and would be able to undergo charge or Dexter energy transfer, leading to a minor impact on efficiency loss.

The NFA triplet yield by SOC-driven ISC is assumed to be low in these OSCs, as demonstrated by a weak trEPR signal in the spin-coated substrates (Figure S2, Supporting Information). However, we additionally confirmed HBT from $|^3CT\rangle$ states formed via non-geminate recombination of free charge carriers, visible in PLDMR spectra of all blends. The origin lies in the recombination of free charge carriers with uncorrelated spin orientation that lead to the formation of 25% CT singlets and 75% CT triplets.[74] The latter can relax spin-allowed to the lowest molecular triplet states via non-geminate HBT (dark red arrows in Figure 5).[17] Thereby, excitons initially occupy the three triplet sublevels equally according to spin statistics, but will gain a small spin polarization due to a combination of spin-lattice relaxation and unequal triplet sublevel decays. Continuous optical excitation in PLDMR further enhances the spin polarization due to accumulation-driven spin-dependent annihilation processes. In combination with the optical detection, this improves the sensitivity to non-geminate triplet excitons

in contrast to trEPR. Gillett et al. showed with TA spectroscopy that in the blend PM6:Y6 ≈90% of the non-geminately recombined CT states undergo HBT to the NFA triplet.[3] In contrast, the ISC yield in neat Y6 is ≈3%, further reduced in the blends due to a significant charge transfer of 90% upon photoexcitation.[3] Regarding the similarity of ISC and hole transfer rates discussed below, we assume similar amounts of triplet excitons from non-geminate recombination in all PBDB-T:Y-series blends, as detected via PLDMR (Figure 2). Furthermore, trPLDMR of PM6:Y6 blend films shows a similar temporal response of the Y6 triplets and the CT states, supporting the population by non-geminate HBT, while Y6 triplets in neat film possess a different time response in agreement with triplets predominantly populated by ISC (Figure S10, Supporting Information). Since the rate of non-geminate HBT is shown to increase with temperature, the presence of non-geminate HBT triplet excitons even at 10 K highlights the importance of this loss channel for solar cells operated at ambient temperatures.[3] For further evidence of dominant non-geminate recombination at room temperature, we measured TA at 293 K in the infrared region, where the formation of the NFA triplet PIA is observable (Figure S3, Supporting Information). The strong fluence-dependence of the Y6 triplet generation in this spectral region attributes the population to a dominating bimolecular/non-geminate recombination in all (non-) halogenated blends, as already identified by PLDMR at low temperatures. These triplet recombinations have been shown to result in a non-radiative voltage loss of up to 60 meV in operational solar cells, with our study implying a similar degree with respect to new donor or acceptor halogenations.[3]

4.2. Impact of Halogenation on Triplet Formation

The number of excitons undergoing the above-mentioned processes additionally depends on the kinetics of the system, whereby the two most important rates affecting the population of triplet states upon initial excitation of the singlet states are hole transfer and ISC rates. As differences in hole transfer kinetics would give the singlet excitons more/less time to undergo ISC, we studied the impact of halogenation on both rate constants. Regarding the halogenation of the acceptor, one could invoke an increase in SOC due to heavier halogen atoms, boosting ISC as has already been shown in literature for bromine or iodine in TADF molecules.[75] However, QC calculations on NFA Y-series reveal that, starting from the non-halogenated acceptor Y5, the ISC rate constant does not change significantly upon fluorination and chlorination in these molecules due to the absence of significant weight on the halogen atoms (see Table S4, Figure S7 for Y6, and Figure S8 for the PM6, Supporting Information). As for the hole transfer kinetics, halogenation of PBDB-T lowers the donor HOMO energy level (Figure S17, Supporting Information), leading to increased V_{OC} in solar cells with PM6 and PM7.[62,76] The smaller energy offset is desirable to minimize energy losses but one could consider an effect on the driving force due to a smaller HOMO offset.[20,67] However, TA measurements (Figure 4b) showed a comparable hole transfer rate constant with the three different (non-) halogenated donors and with both NFAs (Figure S4,

Supporting Information). This outcome is not surprising, as the overall hole transfer rate has been shown not being sensitive to the HOMO offset, especially in low-offset OSC: while the "intrinsic" hole transfer rate of NFA excitons generated in close proximity to the D:A interface occurs on sub-ps timescales, the overall hole transfer process takes place over timescales of tens of picoseconds, depending on exciton diffusion in the bulk morphology.[64] Furthermore, Ma et al. showed that hole transfer rates for PM6:Y6 are only weakly affected by temperature in the range from 15 to 300 K, allowing the comparison with the low-temperature EPR measurements.[73]

However, while the triplet population kinetics upon initial singlet excitation are shown to be comparable for (non-) halogenated donor and acceptor combinations, the number of excitons undergoing these processes is determined to be different. Comparing TA and trEPR for all Y6 blends with substrates prepared in the same way according to the optimized recipe (Figures S1 and S2, Supporting Information), the hole transfer yield decreases upon halogenation, while trEPR data show a detectable ISC yield in PM6:Y6 and PM7:Y6. This result surprisingly suggests a positive effect of using the non-halogenated donor PBDB-T by revealing a reduced triplet exciton yield. As already mentioned, halogenation also impacts the morphology by, e.g., increasing domain sizes due to fluorination or chlorination as a result of a reduced miscibility.[77–79] These increased domain sizes are suggested to lead to a decrease in the number of excitons reaching the D:A interface and instead undergoing ISC in blends with halogenated donor PM6 and PM7. Indeed, Eastham et al. investigated different donor materials with NFA ITIC, demonstrating that efficient hole transfer depends strongly on the blend morphology rather than the energy level alignment.[80] Domain sizes in the range of the exciton diffusion length are normally beneficial for dissociation of charge carriers, improving short-circuit current density and fill factor of the solar cell.[77,78] However, we showed by the analysis of the spin physics in these systems, that triplet recombination pathways can be unfavorably affected. Thus, the key point for a good performing OSC is matching a good trade-off in efficient photophysical processes and beneficial bulk morphology to reduce charge generation losses, as in PBDB-T:Y6, but also beneficial subsequent exciton dissociation, as in PM6:Y6 and PM7:Y6.[81]

There are different design strategies for next-generation OSCs to engineering out the triplet loss pathways: One approach is to reduce the HBT rate to molecular triplet states by hybridization between CT and local excitons or to outcompete triplet recombination by fast charge separation.[3,82] Another approach is the combination of state-of-the-art OPV and OLED research by designing the second OSC component with small singlet-triplet gap, e.g., intramolecular TADF emitters. This combination would generally prevent energetically trapped triplet excitons by thermal reactivation, while simultaneously preserve the small voltage losses.

5. Conclusion

In this work, we applied triplet spin-sensitive techniques (PLDMR, trEPR) together with TA and QC calculations to reveal non-radiative loss processes by triplet excitons. Using

the strengths of these complementary methods, we were able to detect and distinguish various triplet excitons present in the investigated blends and draw a comprehensive picture of their generation pathways. We thereby studied different state-of-the-art donor:acceptor combinations with the (non-) halogenated polymers PBDB-T, PM6, PM7 and the NFAs Y6 and Y7 and detected triplet excitons in all blends. These excitons are energetically trapped on the low-lying NFA triplet states, where they are unable to contribute to OSC performance due to a high energetic gap to CT states. While the major contribution observed in all blends is non-geminate HBT, blends with halogenated donors possess an additional triplet population pathway through SOC-driven ISC on the NFA. The impact of halogenation on the rates affecting the population of triplet states after excitation of the NFA singlet states, in particular ISC and hole transfer, is comparable for all combinations. Thus, shifting of HOMO levels or the presence of heavier halogen atoms have a minor influence on excited states kinetics. However, the increased triplet exciton yield by ISC with best performing PM6 and PM7 indicates an incomplete charge carrier generation, suggesting an adverse impact of domain aggregation through halogenation. While the benefits of halogenation still prevail in terms of overall device efficiency, we uncovered triplet excitons and associated pathways in all these (non-) halogenated blends that clearly show that there is untapped potential for reaching the 20% milestone.

6. Experimental Section

As donor materials, poly[[4,8-bis[5-(2-ethylhexyl)-2-thienyl]benzo[1,2-*b*:4,5-*b′*]dithiophene-2,6-diyl]-2,5-thiophenediyl[5,7-bis(2-ethylhexyl)-4,8-dioxo-4*H*,8*H*-benzo[1,2-*c*:4,5-*c′*]dithiophene-1,3-diyl]po-lymer (PBDB-T), poly[[4,8-bis[5-(2-ethylhexyl)-4-fluoro-2-thienyl]benzo[1,2-*b*:4,5-*b′*]dithiophene-2,6-diyl]-2,5-thiophenediyl[5,7-bis(2-ethylhexyl)-4,8-dioxo-4*H*,8*H*-benzo[1,2-*c*:4,5-*c′*]dithiophene-1,3-diyl]-2,5-thiophenediyl] (PBDB-T-2F or PM6), and poly[[4,8-bis[5-(2-ethylhexyl)-4-chloro-2-thie-nyl]benzo[1,2-*b*:4,5-*b′*]dithiophene-2,6-diyl]-2,5-thiophenediyl[5,7-bis(2-ethylhexyl)-4,8-dioxo-4*H*,8*H*-benzo[1,2-*c*:4,5-*c′*]dithiophene-1,3-diyl]-2,5-thiophenediyl] (PBDB-T-2Cl or PM7) were used. NFAs represent 2,2″-((2Z,2″Z)-((12,13-bis(2-ethylhexyl)-3,9-diundecyl-12,13-dihydro-[1,2,5]thiadiazolo[3,4-e]thieno[2′,3″:4′,5″]thieno[2″,3″:4,5]pyrrolo[3,2-g]thieno[2″,3″:4,5]thieno[3,2-b]indole-2,10-diyl)bis-(methanylylidene))bis(5,6-difluoro-3-oxo-2,3-dihydro-1H-indene-2,1-diylidene))dimalononitrile (BTP-4F or Y6), and 2,2″-((2Z,2″Z)-((12,13-bis(2-ethylhexyl)-3,9-diundecyl-12,13-dihydro-[1,2,5]thiadiazolo-[3,4-e]thieno[2″,3″:4′,5″]thieno[2″,3″:4,5]pyrrolo[3,2-g]thieno[2″,3″:4,5]thieno[3,2-b]indole-2,10-diyl)-bis(methanylylidene))bis(5,6-dichloro-3-oxo-2,3-dihydro-1H-indene-2,1-diylidene))dimalononitrile (BTP-4Cl or Y7). All materials were purchased from 1-materials or Sigma–Aldrich.

Substrates were prepared from solution according to the optimized recipe (18 mg mL^{-1}, 1:1.2 polymer:NFA, dissolved in CF with 1-chloronaphthalene 0.5 v/v%),[37,38] which was spin-coated with 3,000 rpm for 30 s on substrates (10 mm × 10 mm for TA, 20 mm × 20 mm for PLDMR/trEPR) and annealed at 110 °C for 10 min. TA samples were encapsulated under nitrogen atmosphere with 20 mm × 20 mm × 0.2 mm cover glass. Samples for PLDMR and trEPR were cut into strips of 2 mm width, whereby 10 strips were placed in an EPR quartz tube (Wilmad O.D. 4 mm). The sample tubes were sealed under inert helium atmosphere. For EPR measurements on drop-cast samples, materials and blends were dissolved in chlorobenzene (5 mg mL^{-1} for PLDMR, 20 mg mL^{-1} for trEPR) and ≈100 μL were poured into an EPR tube. The solvent was then evaporated by vacuum pumping,

creating a thin film on the EPR tube wall. The sample tubes were also sealed under inert helium atmosphere.

PLDMR and trEPR experiments were carried out with a modified X-band spectrometer (Bruker E300) equipped with a continuous-flow helium cryostat (Oxford ESR 900) and a microwave cavity (Bruker ER4104OR, 9.43 GHz) with optical access. All measurements were performed at $T = 10$ K.

For PLDMR, microwaves were generated with a microwave signal generator (Anritsu MG3694C), amplified to 3 W (microsemi) and guided into the cavity. Optical irradiation was performed with a 473 nm continuous wave laser (Cobolt). PL was detected with a silicon photodiode (Hamamatsu S2281) on the opposite opening of the cavity, using a 561 nm long pass filter to reject the excitation light. The PL signal was amplified by a current/voltage amplifier (Femto DHPCA-100) and recorded by lock-in detector (Ametek SR 7230), referenced by on-off-modulating the microwaves with 517 Hz.

For trEPR, pulsed optical excitation was performed with a Nd:YAG laser (Continuum Minilite II) with 532 nm; pulse length of 5 ns; 15 Hz repetition rate; 2 mJ per pulse. Microwaves were generated and detected with a microwave bridge (Bruker ER047MRP). Measurements were performed with 20 dB attenuation (2 mW). A voltage amplifier (FEMTO DHPVA-200) and a digitizer card (GaGe Razor Express 1642 CompuScope) were used for transient recording. The time resolution is limited to ≈100 ns by the cavity Q factor of ≈2,800. By sweeping the magnetic field, 2D data sets are recorded, where trEPR spectra are averaged from 0.5 to 1.5 μs after laser excitation.

For TA, a setup powered by a Yb amplifier (PHAROS, Light Conversion), operating at 38 kHz and generating 200 fs pulses centered at 1,030 nm with an output of 14.5 W, was used. The ≈200 fs pump pulse was provided by an optical parametric amplifier (Light Conversion ORPHEUS). The probe was provided by a white light supercontinuum generated in a YAG crystal from a small amount of the 1,030 nm fundamental. After passing through the sample, the probe is imaged using a Si photodiode array (Stresing S11490).

QC calculations were carried out by using time-dependent DFT calculations within the Tamm–Dancoff approximation (TDA). For these calculations, optimally tuned screened range-separated hybrid (SRSH) LC-ωhPBE/6-311G(d,p) level of theory was employed, where the scalar dielectric constant was set at 4.5. In addition, SOC matrix elements were computed in the Brett–Pauli spin-orbit Hamiltonian framework as implemented in the PySOC code,[83] performing the calculations at the ωB97X-D/Def2-TZVP level on the NFA Y-series S_1 optimized structure. All calculations were carried out with the Gaussian16 suite.[84] Further details can be found in the Supporting Information.

Supporting Information

Supporting Information is available from the Wiley Online Library or from the author.

Conflict of Interest

The authors declare no conflict of interest.

Author Contributions

J.G., B.S., and S.L. performed the magnetic resonance measurements and evaluated the data. G.L. and Y.O. performed the calculations. A.J.G. performed the transient absorption measurements. J.G. and A.S. wrote the manuscript, which all authors discussed and commented on.

Data Availability Statement

The data that support the findings of this study are available from the corresponding author upon reasonable request.

Keywords

halogenation, non-fullerene acceptors, organic photovoltaics, spin physics, triplet excitons

[1] Y. Lin, J. Wang, Z. G. Zhang, H. Bai, Y. Li, D. Zhu, X. Zhan, *Adv. Mater.* **2015**, *27*, 1170.
[2] Y. Cui, Y. Xu, H. Yao, P. Bi, L. Hong, J. Zhang, Y. Zu, T. Zhang, J. Qin, J. Ren, *Adv. Mater.* **2021**, *33*, 2102420.
[3] A. J. Gillett, A. Privitera, R. Dilmurat, A. Karki, D. Qian, A. Pershin, G. Londi, W. K. Myers, J. Lee, J. Yuan, S.-J. Ko, M. Riede, F. Gao, G. Bazan, A. Rao, T.-Q. Nguyen, D. Beljonne, R. H. Friend, *Nature* **2021**, *597*, 666.
[4] Z. Chen, X. Chen, Z. Jia, G. Zhou, J. Xu, Y. Wu, X. Xia, X. Li, X. Zhang, C. Deng, *Joule* **2021**, *5*, 1832.
[5] J. Hofinger, C. Putz, F. Mayr, K. Gugujonovic, D. Wielend, M. C. Scharber, *Mater. Adv.* **2021**, *2*, 4291.
[6] V. C. Nikolis, J. Benduhn, F. Holzmueller, F. Piersimoni, M. Lau, O. Zeika, D. Neher, C. Koerner, D. Spoltore, K. Vandewal, *Adv. Energy Mater.* **2017**, *7*, 1700855.
[7] J. Benduhn, F. Piersimoni, G. Londi, A. Kirch, J. Widmer, C. Koerner, D. Beljonne, D. Neher, D. Spoltore, K. Vandewal, *Adv. Energy Mater.* **2018**, *8*, 1800451.
[8] W. Shockley, H. J. Queisser, *J. Appl. Phys.* **1961**, *32*, 510.
[9] U. Rau, *Phys. Rev. B* **2007**, *76*, 085303.
[10] X. Wan, C. Li, M. Zhang, Y. Chen, *Chem. Soc. Rev.* **2020**, *49*, 2828.
[11] S. Karuthedath, J. Gorenflot, Y. Firdaus, N. Chaturvedi, C. S. De Castro, G. T. Harrison, J. I. Khan, A. Markina, A. H. Balawi, T. A. D. Peña, *Nat. Mater.* **2021**, *20*, 378.
[12] W. Chang, D. N. Congreve, E. Hontz, M. E. Bahlke, D. P. McMahon, S. Reineke, T. C. Wu, V. Bulović, T. Van Voorhis, M. A. Baldo, *Nat. Commun.* **2015**, *6*, 6415.
[13] T. Ford, I. Avilov, D. Beljonne, N. Greenham, *Phys. Rev. B* **2005**, *71*, 125212.
[14] I. Ramirez, A. Privitera, S. Karuthedath, A. Jungbluth, J. Benduhn, A. Sperlich, D. Spoltore, K. Vandewal, F. Laquai, M. Riede, *Nat. Commun.* **2021**, *12*, 471.
[15] J. Shinar, *Synth. Met.* **1996**, *78*, 277.
[16] S. A. Thomson, J. Niklas, K. L. Mardis, C. Mallares, I. D. Samuel, O. G. Poluektov, *J. Phys. Chem. C* **2017**, *121*, 22707.
[17] A. Rao, P. C. Chow, S. Gélinas, C. W. Schlenker, C.-Z. Li, H.-L. Yip, A. K.-Y. Jen, D. S. Ginger, R. H. Friend, *Nature* **2013**, *500*, 435.
[18] T. Offermans, P. A. van Hal, S. C. Meskers, M. M. Koetse, R. A. Janssen, *Phys. Rev. B* **2005**, *72*, 045213.
[19] V. Dyakonov, N. Gauss, G. Rösler, S. Karg, W. Rieß, M. Schwoerer, *Chem. Phys.* **1994**, *189*, 687.
[20] R. Wang, J. Yuan, R. Wang, G. Han, T. Huang, W. Huang, J. Xue, H. C. Wang, C. Zhang, C. Zhu, *Adv. Mater.* **2019**, *31*, 1904215.
[21] J. Han, X. Wang, D. Huang, C. Yang, R. Yang, X. Bao, *Macromolecules* **2020**, *53*, 6619.
[22] L. Ma, H. Yao, J. Wang, Y. Xu, M. Gao, Y. Zu, Y. Cui, S. Zhang, L. Ye, J. Hou, *Angew. Chem.* **2021**, *60*, 15988.
[23] Y. Xiang, Y. Zhao, N. Xu, S. Gong, F. Ni, K. Wu, J. Luo, G. Xie, Z.-H. Lu, C. Yang, *J. Mater. Chem. C* **2017**, *5*, 12204.
[24] Q. Fan, U. A. Méndez-Romero, X. Guo, E. Wang, M. Zhang, Y. Li, *Chem. Asian J.* **2019**, *14*, 3085.
[25] M. S. Kotova, G. Londi, J. Junker, S. Dietz, A. Privitera, K. Tvingstedt, D. Beljonne, A. Sperlich, V. Dyakonov, *Mater. Horiz.* **2020**, *7*, 1641.
[26] J. Grüne, V. Dyakonov, A. Sperlich, *Mater. Horiz.* **2021**, *8*, 2569.
[27] I. Sudakov, M. Van Landeghem, R. Lenaerts, W. Maes, S. Van Doorslaer, E. Goovaerts, *Adv. Energy Mater.* **2020**, *10*, 2002095.
[28] H. Kraus, M. C. Heiber, S. Väth, J. Kern, C. Deibel, A. Sperlich, V. Dyakonov, *Sci. Rep.* **2016**, *6*, 29158.
[29] A. Privitera, J. Grüne, A. Karki, W. K. Myers, V. Dyakonov, T. Q. Nguyen, M. K. Riede, R. H. Friend, A. Sperlich, A. J. Gillett, *Adv. Energy Mater.* **2022**, *12*, 2103944.
[30] E. Goovaerts, *eMagRes* **2007**, *6*, 343.
[31] S. Väth, K. Tvingstedt, M. Auth, A. Sperlich, A. Dabuliene, J. V. Grazulevicius, P. Stakhira, V. Cherpak, V. Dyakonov, *Adv. Opt. Mater.* **2017**, *5*, 1600926.
[32] T. Biskup, *Front Chem* **2019**, *7*, 10.
[33] S. Weber, *eMagRes* **2007**, *6*, 255.
[34] S. Richert, C. E. Tait, C. R. Timmel, *J. Magn. Reson.* **2017**, *280*, 103.
[35] G. Jeschke, *Macromol. Rapid Commun.* **2002**, *23*, 227.
[36] S. S. Eaton, K. M. More, B. M. Sawant, G. R. Eaton, *J. Am. Chem. Soc.* **1983**, *105*, 6560.
[37] R. Ma, T. Yang, Y. Xiao, T. Liu, G. Zhang, Z. Luo, G. Li, X. Lu, H. Yan, B. Tang, *Energy Environ. Mater.* **2021**, *5*, 977.
[38] F. D. Eisner, M. Azzouzi, Z. Fei, X. Hou, T. D. Anthopoulos, T. J. S. Dennis, M. Heeney, J. Nelson, *J. Am. Chem. Soc.* **2019**, *141*, 6362.
[39] S. Stoll, A. Schweiger, *J. Magn. Reson.* **2006**, *178*, 42.
[40] J. De Ceuster, E. Goovaerts, A. Bouwen, V. Dyakonov, *Phys. Rev. B* **2003**, *68*, 125202.
[41] J. Shinar, *Laser Photon. Rev.* **2012**, *6*, 767.
[42] F. Zhao, K. Wang, J. Duan, X. Zhu, K. Lu, C. Zhao, C. Zhang, H. Yu, B. Hu, *Sol. RRL* **2019**, *3*, 1900063.
[43] Y. Wang, A. Privitera, G. Londi, A. Sneyd, D. Qian, Y. Olivier, L. Sorace, D. Beljonne, Z. Li, A. Gillett, arXiV preprint arXiv:2112.09562, **2021**.
[44] R. Wang, C. Zhang, Q. Li, Z. Zhang, X. Wang, M. Xiao, *J. Am. Chem. Soc.* **2020**, *142*, 12751.
[45] M.-K. Lee, M. Segal, Z. Soos, J. Shinar, M. Baldo, *Phys. Rev. Lett.* **2005**, *94*, 137403.
[46] P. J. Budden, L. R. Weiss, M. Müller, N. A. Panjwani, S. Dowland, J. R. Allardice, M. Ganschow, J. Freudenberg, J. Behrends, U. H. Bunz, R. H. Friend, *Nat. Commun.* **2021**, *12*, 1527.

[47] B. Z. Tedlla, F. Zhu, M. Cox, B. Koopmans, E. Goovaerts, *Phys. Rev. B* **2015**, *91*, 085309.

[48] T. Biskup, M. Sommer, S. Rein, D. L. Meyer, M. Kohlstädt, U. Würfel, S. Weber, *Angew. Chem., Int. Ed.* **2015**, *54*, 7707.

[49] L. Zhu, M. Zhang, G. Zhou, T. Hao, J. Xu, J. Wang, C. Qiu, N. Prine, J. Ali, W. Feng, *Adv. Energy Mater.* **2020**, *10*, 1904234.

[50] G. Zhang, X.-K. Chen, J. Xiao, P. C. Chow, M. Ren, G. Kupgan, X. Jiao, C. Chan, X. Du, R. Xia, Z. Chen, J. Yuan, Y. Zhang, S. Zhang, Y. Liu, H. Yan, K. S. Wong, V. Coropceanu, N. Li, C. J. Brabec, J.-L. Bredas, H.-L. Yip, Y. Cao, *Nat. Commun.* **2020**, *11*, 3943.

[51] Y. Li, H. Meng, J. Huang, C. Zhan, *ACS Appl. Mater. Interfaces* **2020**, *12*, 50541.

[52] J. Yuan, Y. Zhang, L. Zhou, G. Zhang, H.-L. Yip, T.-K. Lau, X. Lu, C. Zhu, H. Peng, P. A. Johnson, *Joule* **2019**, *3*, 1140.

[53] A. Karki, J. Vollbrecht, A. L. Dixon, N. Schopp, M. Schrock, G. M. Reddy, T. Q. Nguyen, *Adv. Mater.* **2019**, *31*, 1903868.

[54] V. Vohra, K. Kawashima, T. Kakara, T. Koganezawa, I. Osaka, K. Takimiya, H. Murata, *Nat. Photon.* **2015**, *9*, 403.

[55] C. Grieco, G. S. Doucette, R. D. Pensack, M. M. Payne, A. Rimshaw, G. D. Scholes, J. E. Anthony, J. B. Asbury, *J. Am. Chem. Soc.* **2016**, *138*, 16069.

[56] Y. Zhang, S. R. Forrest, *Chem. Phys. Lett.* **2013**, *590*, 106.

[57] E. Hontz, W. Chang, D. N. Congreve, V. Bulović, M. A. Baldo, T. Van Voorhis, *J. Phys. Chem. C* **2015**, *119*, 25591.

[58] A. J. Gillett, C. Tonnelé, G. Londi, G. Ricci, M. Catherin, D. M. L. Unson, D. Casanova, F. Castet, Y. Olivier, W. M. Chen, E. Zaborova, E. W. Evans, B. H. Drummond, P. J. Conaghan, L.-S. Cui, N. C. Greenham, Y. Puttisong, F. Fages, D. Beljonne, R. H. Friend, *Nat. Commun.* **2021**, *12*, 6640.

[59] D. Beljonne, Z. Shuai, G. Pourtois, J. Bredas, *J. Phys. Chem. A* **2001**, *105*, 3899.

[60] E. W. Evans, Y. Olivier, Y. Puttisong, W. K. Myers, T. J. Hele, S. M. Menke, T. H. Thomas, D. Credgington, D. Beljonne, R. H. Friend, *J. Phys. Chem. Lett.* **2018**, *9*, 4053.

[61] A. Karki, J. Vollbrecht, A. J. Gillett, S. S. Xiao, Y. Yang, Z. Peng, N. Schopp, A. L. Dixon, S. Yoon, M. Schrock, *Energy Environ. Sci.* **2020**, *13*, 3679.

[62] L. Qin, X. Liu, X. Zhang, J. Yu, L. Yang, F. Zhao, M. Huang, K. Wang, X. Wu, Y. Li, *Angew. Chem., Int. Ed.* **2020**, *59*, 15043.

[63] R. Ma, T. Liu, Z. Luo, Q. Guo, Y. Xiao, Y. Chen, X. Li, S. Luo, X. Lu, M. Zhang, *Sci. China Chem.* **2020**, *63*, 325.

[64] Y. Zhong, M. Causa, G. J. Moore, P. Krauspe, B. Xiao, F. Günther, J. Kublitski, R. Shivhare, J. Benduhn, E. BarOr, S. Mukherjee, K. M. Yallum, J. Rehault, S. C. B. Mannsfeld, D. Neher, L. J. Richter,

D. M. DeLongchamp, F. Ortmann, K. Vandewal, E. Zhou, N. Banerji, *Nat. Commun.* **2020**, *11*, 833.

[65] S. Natsuda, T. Saito, R. Shirouchi, Y. Sakamoto, T. Takeyama, Y. Tamai, H. Ohkita, *Energy Environ. Sci.* **2022**, *15*, 1545.

[66] F. Liu, L. Zhou, W. Liu, Z. Zhou, Q. Yue, W. Zheng, R. Sun, W. Liu, S. Xu, H. Fan, *Adv. Mater.* **2021**, *33*, 2100830.

[67] J. Wu, J. Lee, Y.-C. Chin, H. Yao, H. Cha, J. Luke, J. Hou, J.-S. Kim, J. R. Durrant, *Energy Environ. Sci.* **2020**, *13*, 2422.

[68] S. Refaely-Abramson, S. Sharifzadeh, N. Govind, J. Autschbach, J. B. Neaton, R. Baer, L. Kronik, *Phys. Rev. Lett.* **2012**, *109*, 226405.

[69] S. Hirata, M. Head-Gordon, *Chem. Phys. Lett.* **1999**, *314*, 291.

[70] S. Lower, M. El-Sayed, *Chem. Rev.* **1966**, *66*, 199.

[71] M. A. El-Sayed, *Acc. Chem. Res.* **1968**, *1*, 8.

[72] G. Han, T. Hu, Y. Yi, *Adv. Mater.* **2020**, *32*, 2000975.

[73] C. Ma, C. C. Chan, X. Zou, H. Yu, J. Zhang, H. Yan, K. S. Wong, P. C. Chow, *Sol. RRL* **2021**, *5*, 2000789.

[74] S. M. Menke, A. Sadhanala, M. Nikolka, N. A. Ran, M. K. Ravva, S. Abdel-Azeim, H. L. Stern, M. Wang, H. Sirringhaus, T.-Q. Nguyen, *ACS Nano* **2016**, *10*, 10736.

[75] J. Wang, X. Gu, H. Ma, Q. Peng, X. Huang, X. Zheng, S. H. Sung, G. Shan, J. W. Lam, Z. Shuai, B. Z. Tang, *Nat. Commun.* **2018**, *9*, 2963.

[76] Q. Fan, Q. Liu, W. Gao, Y. Xiao, J. Wu, W. Su, X. Guo, X. Lu, C. Yang, H. Yan, *J. Mater. Chem. A* **2019**, *7*, 15404.

[77] Q. Fan, Q. Zhu, Z. Xu, W. Su, J. Chen, J. Wu, X. Guo, W. Ma, M. Zhang, Y. Li, *Nano Energy* **2018**, *48*, 413.

[78] R. Ma, G. Li, D. Li, T. Liu, Z. Luo, G. Zhang, M. Zhang, Z. Wang, S. Luo, T. Yang, *Sol. RRL* **2020**, *4*, 2000250.

[79] Z. Liu, Y. Gao, J. Dong, M. Yang, M. Liu, Y. Zhang, J. Wen, H. Ma, X. Gao, W. Chen, *J. Phys. Chem. Lett.* **2018**, *9*, 6955.

[80] N. D. Eastham, J. L. Logsdon, E. F. Manley, T. J. Aldrich, M. J. Leonardi, G. Wang, N. E. Powers-Riggs, R. M. Young, L. X. Chen, M. R. Wasielewski, *Adv. Mater.* **2018**, *30*, 1704263.

[81] G. Dennler, M. C. Scharber, C. J. Brabec, *Adv. Mater.* **2009**, *21*, 1323.

[82] P. C. Chow, C. C. Chan, C. Ma, X. Zou, H. Yan, K. S. Wong, *J. Phys. Chem. Lett.* **2021**, *12*, 5045.

[83] X. Gao, S. Bai, D. Fazzi, T. Niehaus, M. Barbatti, W. Thiel, *J. Chem. Theory Comput.* **2017**, *13*, 515.

[84] M. J. Frisch, G. W. Trucks, H. B. Schlegel, G. E. Scuseria, M. A. Robb, J. R. Cheeseman, G. Scalmani, V. Barone, G. A. Petersson, H. Nakatsuji, X. Li, M. Caricato, A. V. Marenich, J. Bloino, B. G. Janesko, R. Gomperts, B. Mennucci, H. P. Hratchian, J. V. Ortiz, A. F. Izmaylov, J. L. Sonnenberg, Williams, F. D., F. Lipparini, F. Egidi, J. Goings, B. Peng, A. Petrone, T. Henderson, D. Ranasinghe, et al., Gaussian, Inc., Wallingford CT, **2016**.